ORNL/TM-2018/2

Coupled Mass and Heat Transport Models for Nuclear Fuels using Thermodynamic Calculations

S. Simunovic
J. W. McMurray
T. M. Besmann
E. E. Moore
M. H. A. Piro

31 October 2017

OAK RIDGE NATIONAL LABORATORY
MANAGED BY UT-BATTELLE FOR THE US DEPARTMENT OF ENERGY

ORNL/TM-2018/2

Computer Science and Mathematics Division

COUPLED MASS AND HEAT TRANSPORT MODELS FOR NUCLEAR FUELS USING THERMODYNAMIC CALCULATION

S. Simunovic[1]
J. W. McMurray[1]
T. M. Besmann[2]
E. Moore[2]
M. H. A. Piro[3]

[1]Oak Ridge National Laboratory, Oak Ridge, TN
[2]University of South Carolina, Columbia, SC
[3]University of Ontario Institute of Technology, Oshawa, ON, Canada

Date Published: October 31, 2017

Prepared by
OAK RIDGE NATIONAL LABORATORY
Oak Ridge, TN 37831-6283
managed by
UT-BATTELLE, LLC
for the
US DEPARTMENT OF ENERGY
under contract DE-AC05-00OR22725

CONTENTS

ABSTRACT

We have developed a theoretical framework for incorporation of thermodynamic equilibrium calculations into engineering models of nuclear fuel problems based on the finite element method (FEM). The framework is based on linear irreversible thermodynamics and their incorporation into integral equations for balancing energy and mass. For coupled energy and mass transport, thermodynamic calculations are performed at the nodal points of the FEM mesh and are used at the integration points to calculate the driving forces and fluxes for irreversible thermodynamic problems. The consistent coupling of thermodynamic models with isotopic calculations and other nuclear fuel physics models has been described. The approach has been demonstrated on simple unit problems. Implementation in practical nuclear fuel problems will be developed follow-on research.

1. INTRODUCTION

The evolving composition of the uranium dioxide nuclear fuel in nuclear power reactors during irradiation has a strong effect on the performance and safety of nuclear fuel elements [1]. The composition and associated chemical reactions influence the fuel's thermo-mechanical properties, such as thermal conductivity, specific heat, coefficient of thermal expansion, microstructure, and a variety of transport and diffusion controlled properties [2]. The chemical reactions between the volatile fission products and the fuel cladding can also limit the performance of fuel elements.

The changing nuclear fuel composition during irradiation is driven by the nuclear fission processes, chemical reactions, and heat and mass transport that occur under large thermal gradients and composition variations. Due to severe limitations of in-situ monitoring of fuel composition and the complexity of modeling multicomponent systems, fuel thermo-chemical models are usually derived from experiments on fresh or simulated irradiated fuel, which may rely on the assumption of a single UO_2 solid solution phase. However, as the irradiation and fuel burnup progresses, several new phases may form due to the creation of fission products and their interactions with the fuel matrix phase [3, 4]. The current thermodynamic computation library, Thermochimica [5], provides a unique capability of computing the spatial distribution of phases across the nuclear fuel pellet with burnup. Figure 1 shows the changes in all phases in the radial direction at a burnup of 102 $GW \cdot d \cdot t(U)^{-1}$ based on the experiments from reference [6].

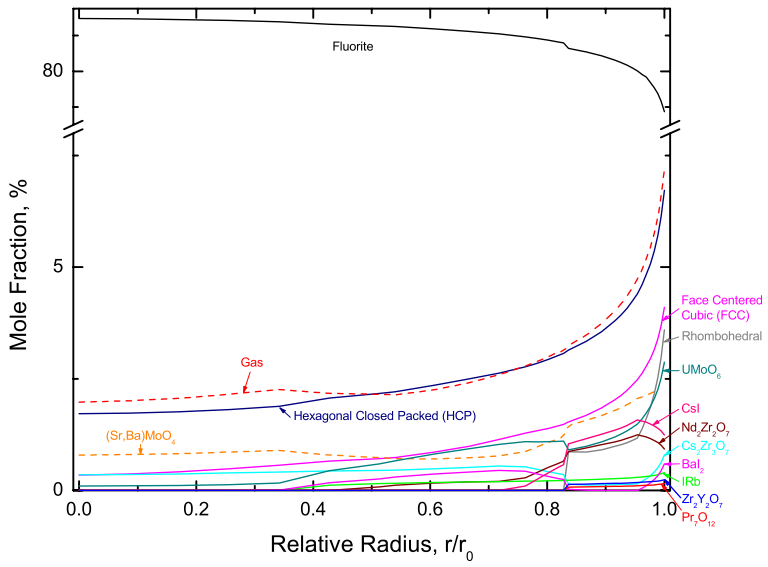

Figure 1. The predicted distribution of phases across the pellet at a burnup of 102 GW·d·t(U)$^{-1}$[4].

As is to be expected, the fluorite oxide phase is the dominant phase and several additional minor phases are predicted to be stable, including noble metal inclusions in the face centered cubic and hexagonal closed packed crystal structures, other oxides, and gas. The co-existence of these phases is important in computing the oxygen-to-metal ratio and the oxygen chemical potential. The fission and radioactive decay products, together with high temperatures result in the formation of structural defects in the primary fuel phase. These defects in the UO_2 lattice control a wide range of phenomena in the nuclear fuel. The main types of structural disorder created by fission and high temperatures are the formation of Frenkel defectson the anion, oxygen, sub-lattice [7]. Schottky defects are less prevalent and occur on both anion and cation sub-lattices. Mass transport occurs primarily through coordinated movement of defects on the anion lattice, whereas the movement on the cation (i.e., uranium) lattice is much slower but significant enough to control the creep rate by movement of uranium vacancies. The fuel's oxidation state and the oxygen chemical potential are considered to be the most important chemical properties [8] of the nuclear fuel as they affect almost all the processes of practical importance. The temperature and the oxygen chemical potential determine the chemical form of the fission products [9], e.g. whether they are stable as a metal or an oxide, dissolve in the fuel matrix or form new phases, etc. The non-uniformity of oxygen potential results in oxygen migration through the fuel and can lead to heterogeneity of the material composition and properties.

To account for all these processes, it is necessary to develop sophisticated thermo-chemical models for the uranium dioxide fuel composition and integrate them with other nuclear fuel performance models. Of primary interest are the heat transport and mass diffusion models. The thermodynamic equilibrium models can provide material properties and the driving forces for these dissipative, non-equilibrium processes. The thermodynamic equilibrium models do not provide the rate of chemical reactions as they only calculate the resulting state for a given mass for each component, pressure and temperature. However, the high temperatures and long-time intervals of the steady power generation in nuclear fuel make the equilibrium models a reasonable approximation of reality.

Thermodynamic equilibrium calculations can be computationally expensive when integrated into a multi-physics framework, which is due to the fact that a nested iterative optimization operation is required at every point in space and time [5, 10]. Therefore, thermodynamic evaluations are to be kept at minimum in order not to overwhelm other physics models. Special constraints on the thermodynamic calculations (i.e.,

chemical potential gradient at constant temperature) are expensive and not well defined in the methods based on a discretized continuum, such as FEM. In addition, the fuel experiences extremely large temperature gradients (90-160 °C/mm) and varying chemical composition, so that separating the two effects is not straightforward.

In the following, we outline the formulation for coupled models for heat and mass transport, and integrate them with thermodynamic equilibrium models using an irreversible thermodynamics framework and FEM. The models are primarily focused on nuclear fuel elements, but the formulation can be extended to other situations with large thermal and compositional gradients. The main objective of the formulation is to incorporate thermodynamic equilibrium calculations into coupled, multi-physics heat and mass transport models without incurring substantial penalty in computation time. The expected benefits are a more consistent problem formulation, models for the material composition in multi-component systems, and a better approximation of the driving forces and fluxes for irreversible processes. The formulations as of now only provide the foundation for a framework for including thermodynamic calculations and will need to be further developed in ongoing research.

2. IRREVERSIBLE THERMODYNAMICS OF MASS AND HEAT TRANSPORT IN CHEMICALLY REACTING MEDIUM

Thermodynamic models calculate the composition, chemical and physical properties of a material system that is in equilibrium [11]. The Gibbs energy is at a minimum at constant temperature and pressure, with no entropy production and no thermodynamic forces operating within the system. However, heat and mass transport are non-equilibrium dissipative processes, driven by the unbalanced driving forces. The processes considered here are assumed to occur on sufficiently large time increments to be treated as having another type of time-independence, a steady-state [12]. The systems are open and can exchange energy and mass with the environment. Constant driving forces result in stationary fluxes and stationary states. For example, the temperature or composition profile does not change during the steady-state conditions, although the entropy is being produced in the system. The constant driving forces and fluxes result in the ultimate steady state of the irreversible systems, which can be described with equilibrium thermodynamics models. In effect, equilibrium thermodynamics is used to model kinetic, non-equilibrium phenomena [13]. It is implicitly assumed that the system is sufficiently near equilibrium that there is a linear relation between the driving forces and rate processes. These assumptions are less restrictive in transport models which assume that the gradients are not too large than they are for chemical reaction models.

Heat and mass transport simulations are usually cast in the framework of irreversible thermodynamics. The method is based on the assumption of local equilibrium in the constitutive volumes, and conservation laws for energy and mass balance in the system. The macro non-equilibrium system is assumed to be an assembly of open elemental volumes that are in equilibrium and thus equilibrium thermodynamic relations are valid for locally defined thermodynamic variables. The elemental volumes can be used to describe heterogeneous systems as long as temperatures, T, can be well-defined at every location. The intensive thermodynamic variables, temperature (T), pressure, (p) and chemical potential of substance k (μ_k), become functions of position $\boldsymbol{x}$, and time, t:

$$T = T(\boldsymbol{x}, t) \quad , \quad p = p(\boldsymbol{x}, t) \quad , \quad \mu_k = \mu_k(\boldsymbol{x}, t) \tag{1}$$

The extensive thermodynamic variables are replaced by their volumetric densities as:

$$s = s(\boldsymbol{x}, t) \quad , \quad u = u(\boldsymbol{x}, t) \quad , \quad n_k = n_k(\boldsymbol{x}, t) \tag{2}$$

where *s, u*, and n_k denote entropy per unit volume, internal energy per unit volume and moles per unit volume of substance k, respectively.
Integrated values of the densities over the system volume do not mutually correlate by standard thermodynamic equilibrium relations because the system is not in equilibrium. However, the local thermodynamic equilibrium relations are valid as long as temperature and composition are well defined for each point in space and time.

The second law of thermodynamics is formulated in terms of entropy production in the form of internally generated heat. Starting from the time rate of the Gibbs relation [14]:

$$T\frac{ds}{dt} = \frac{du}{dt} - \sum_k \mu_k \frac{dn_k}{dt} \tag{3}$$

Assuming the absence of pressure-volume effects, and combining it with the conservation of energy and conservation of mass equations, we can cast the result in the form of an entropy balance equation:

$$\frac{ds}{dt} + \nabla \cdot J_s = \sigma \tag{4}$$

where divergence of the entropy flux for constant pressure system, J_s, is:

$$J_s = \frac{J_h}{T} - \sum_k \frac{\mu_k}{T} J_k \tag{5}$$

where J_h, and J_k denote flux of enthalpy and flux of substance *k*, respectively. Equation (4) represents the rate of exchange of entropy of a local system with its surroundings. This exchange is not the only effect on the local entropy change. The change is influenced by the local, internal entropy production density, σ. Under constant pressure, the local entropy production is:

$$\sigma = J_h \cdot \nabla\left(\frac{1}{T}\right) - \sum_k J_k \cdot \nabla\left(\frac{\mu_k}{T}\right) + \sum_j \frac{A_j v_j}{T} \geq 0 \tag{6}$$

A_j and v_j denote the affinity and the velocity of reaction *j*. In equation (6), the flux of enthalpy, J_h, is composed of the heat current density, J_q, and the mass action current density, J_m, as:

$$J_h = J_q + J_m = TJ_s + \sum_k \mu_k J_k \tag{7}$$

There are many equivalent expressions for defining the heat flow in the coupled heat and mass transport models [15]:

$$J_h = J_q'' + \sum_k h_k J_k \quad , \quad J_u = J_q' + \sum_k u_k J_k \tag{8}$$

Here, J_q'' and J_q' denote two different forms for heat flux. The specific form is selected based on physical conditions and measurements. The partial molar quantities of the diffusing species in the above relations, u_k , h_k, and s_k denote the partial internal energy density, partial molar enthalpy density and partial molar entropy density of the diffusing substance, *k*, i.e.:

$$s_k = \left(\frac{\partial s}{\partial n_k}\right) \quad , \quad u_k = \left(\frac{\partial u}{\partial n_k}\right) \quad , \quad h_k = \left(\frac{\partial h}{\partial n_k}\right) \tag{9}$$

For fixed pressure, the partial molar properties are related as:

$$h_k = \mu_k + s_k \mathrm{T} \tag{10}$$

The equation for internal entropy production density, σ, is the starting expression for developing models of irreversible thermodynamics. It has a general form of a sum of products of conjugate thermodynamic forces and fluxes describing the underlying irreversible processes. Both energy and mass fluxes work to diminish (act conjugate to) spatial gradients of their respective intensive state variables, i.e., driving forces. It is common to select first thermodynamic fluxes as physical, measurable quantities that are part of balance equations, and then select the conjugate quantities as the driving forces. We can also start from selection of driving forces as gradients of intensive variables and then select conjugate flux terms. Both approaches are generally valid as long as the entropy production rate remains invariant.

In equation (6), the force $\nabla\left(\frac{1}{T}\right)$ drives the flow of enthalpy, J_h, that includes the effects of heat and matter flow. The force $\nabla\left(\frac{\mu_k}{T}\right)$ drives mass diffusion, J_k, and the force $\frac{A_j}{T}$ drives the flow of ν_j chemical reaction *j*. In isothermal, dilute systems, the concentration correlates with the chemical potential and the driving force is commonly expressed by Fick's law. However, a multicomponent, multiphase, reacting system of nuclear fuel undergoing burnup at large thermal gradients and composition does not fit those assumptions. Mass diffusion is driven by the decrease in free energy and reducing the chemical potential difference. It shows that diffusion is always along the negative gradient of the Planck potential $\frac{\mu_k}{T}$, which includes effects of composition variation, temperature, and – to a lesser extent – pressure.

The driving forces in equation (6) are not fully decoupled since the chemical potential gradient also contains a temperature gradient. Equation (6) can be transformed to derive its alternative forms in order to differently group the forces and fluxes. To separate the temperature from the chemical potential gradient term in equation (6), we can first take the gradient of the quotient:

$$\nabla\left(\frac{\mu_k}{T}\right) = \frac{1}{T}\nabla\mu_k + \mu_k\nabla\left(\frac{1}{T}\right) \tag{11}$$

or equivalently:

$$\nabla\left(\frac{\mu_k}{T}\right) = \frac{1}{T}\nabla\mu_k - \frac{\mu_k}{T^2}\,\nabla T \tag{12}$$

where the gradients on the right-hand side do not have restrictions of constant temperature or composition. In equations (11) and (12), the gradient of chemical potential still contains the gradient of temperature since $\mu_k(T, p, n_k)$ is a function of temperature, pressure, and composition.

Separation of the temperature gradient and isothermal chemical gradient (i.e., due to compositional variation only) gives:

$$\nabla\left(\frac{\mu_k}{T}\right) = \frac{1}{T}\nabla(\mu_k)_T + h_k\nabla\left(\frac{1}{T}\right) \quad (13)$$

$$\nabla\mu_k = \nabla(\mu_k)_T - s_k\nabla\mathrm{T} \quad (14)$$

Substituting equation (13) in the expression for the entropy production in equation (6) yields:

$$\sigma = J_q'' \cdot \nabla\left(\frac{1}{T}\right) - \sum_k J_k \cdot \frac{\nabla(\mu_k)_T}{T} \quad (15)$$

Either equation (6) or (15), can be used to model the coupled systems of heat transport and mass diffusion, and select the corresponding pairs of forces and fluxes. The choice is usually based on which form provides for easier computational implementation and experimental measurement of the parameters. Historically, equation (15) has been used in coupled thermo-diffusion problems to define the driving forces and fluxes, and to identify the form of the Onsager equations.

3. PHENOMENOLOGICAL MODELS FOR THE MASS AND ENERGY TRANSPORT IN CHEMICALLY REACTING MEDIUM

In linear irreversible thermodynamics, the fluxes are linearly proportional to the driving forces and the proportionality factors are phenomenological expressions that do not depend on the gradient values of the thermodynamic variables. In the linear regime, the system evolves to stationary, steady state with a constant entropy production. When fluxes and generalized to include coupling terms of the same dimensionality, the proportionality coefficients L_{ij} couple all the driving forces as:

$$J_i = \sum L_{ij}F_j = \mathbf{L}\,\mathbf{F} \quad (16)$$

which form an Onsager [16] matrix, **L**, and a vector of driving forces, **F**. This matrix is symmetric and its coefficients, L_{ij}, describe contributions to flux J_i by unit force F_j per Onsager reciprocity theorem. The coefficients are kinetic parameters, independent of the forces acting at the point regardless of their nature (i.e., diffusional, electrical, thermal, mechanical, etc.), and depend only on temperature and composition.

For diffusion of a single component, *k*, coupled with the enthalpy transport, the Onsager equations based on equation (6) become:

$$J_h = L_{hh}\nabla\left(\frac{1}{T}\right) - L_{hk}\nabla\left(\frac{\mu_k}{T}\right) \quad (17a)$$

$$J_k = L_{kh}\nabla\left(\frac{1}{T}\right) - L_{kk}\nabla\left(\frac{\mu_k}{T}\right) \quad (17b)$$

Using the forces and fluxes from equation (15), the Onsager equations are:

$$J_q'' = L_{qq}\nabla\left(\frac{1}{T}\right) - L_{qk}\frac{\nabla(\mu_k)_T}{T} \quad (18a)$$

$$J_k = L_{kq}\nabla\left(\frac{1}{T}\right) - L_{kk}\frac{\nabla(\mu_k)_T}{T} \quad (18b)$$

The equivalence of the two forms can be derived from the physical interpretation of the first pair of equations (17). The foregoing equations use the flux of enthalpy, J_h, which is a variable that describes the state of the system. There are no mechanisms operating on enthalpy that would make it flow through the system even though the above equations formally established the phenomenon. The enthalpy flux equation (17a) can be used to derive the heat flux equation, which is a more fundamental physical phenomenon. Defining the heat flux by subtracting enthalpy of the moving matter from the total enthalpy flux:

$$J_q^* = J_h - h_k J_k \quad (19)$$

and keeping the matter flux the same, $J_k^* = J_k$, in order to keep the entropy production, σ, invariant, results in new force terms:

$$F_q^* = \nabla\left(\frac{1}{T}\right) \quad (20a)$$

$$F_k^* = -\nabla\left(\frac{\mu_k}{T}\right) + h_k\nabla\left(\frac{1}{T}\right) = -\frac{1}{T}\nabla(\mu_k)_T \quad (20b)$$

where the last equality in equation (20b) results from equation (13). Therefore, $J_q^* = J_q''$, and the principal driving force for mass flux is $\nabla(\mu_k)_T$, i.e., the variation of chemical potential due to a gradient in composition.

Using $\nabla(\mu_k)_T$ as the driving force in FEM simulations is difficult because a thermodynamic equilibrium solver calculates the chemical potentials at the finite element nodes while the fluxes and gradients are calculated at the finite element integration points based on the nodal values. The temperatures at the nodes may vary, so that the gradient of the chemical potential at the integration point would include the effects of varying temperature. Therefore, $\nabla\left(\frac{\mu_k}{T}\right)$, or $\nabla\mu_k$, would be preferred driving forces to avoid ambiguity of defining $\nabla(\mu_k)_T$ [17] The transformation of the phenomenological coefficients between the equations based on J_h and J_q'' can be established using equations (18) and (20) to relate to the measured values available in the literature.

The equation for coupled thermo-diffusion mass flux derived from equations (18) is usually given in the literature [18-22], as:

$$J_k = -L_{kk}\left[\nabla(\mu_k)_T - Q_k^{*\prime}\frac{\nabla T}{T}\right] \quad (21)$$

where the effect of thermal gradient on diffusion uses the concept of reduced (i.e., effective) heat of transport, $Q_k^{*\prime}$, which has not been resolved experimentally or theoretically [19, 23, 24]. Some interpretations include dependencies on gradients of thermodynamic quantities which is not in line with the tenets of linear irreversible thermodynamics. In some studies of $UO_{2\pm x}$ [25-27], it was shown that the

reduced heat of transport correlates to the negative partial molar enthalpy of the diffusing species, $-h_k$, in which case the equation (17) recovers the form of equation (18).
For this to be significant for the assumed uncoupled processes of mass and heat transport, the thermodynamic force for the mass flux in equation (17) is expressed as:

$$F_k = -\mathrm{T}\,\nabla\left(\frac{\mu_k}{T}\right) = -\mathrm{T}\,\left(\frac{1}{T}\nabla(\mu_k)_T + h_k\nabla\left(\frac{1}{T}\right)\right) \quad (22)$$

$$F_k = -\nabla(\mu_k)_T + h_k\frac{\nabla T}{T} \quad (23)$$

The corresponding flux is proportional to the driving force:

$$J_k = -L_{kk}\left[\nabla(\mu_k)_T - h_k\frac{\nabla T}{T}\right] \quad (24)$$

which gives $Q_k^{*\prime} = -h_k$.

Assuming the coupling of the gradient of the Planck potential and temperature gradient using equation (17), the equivalent flux relation in terms of Onsager coefficients is defined in the literature [28] as:

$$J_k = -L_{kk}\left[T\nabla\left(\frac{\mu_k}{T}\right) + Q_k^*\frac{\nabla T}{T}\right] \quad (25)$$

where Q_k^* is called the heat of transport. Its relation to the reduced heat of transport is given by:

$$Q_k^{*\prime} = Q_k^* - h_k \quad (26)$$

The assumption in the above referenced studies is that the heat of transport is negligible compared to the partial molar enthalpy of the diffusing substance. Therefore, using the driving force $\nabla\left(\frac{\mu_k}{T}\right)$ for mass diffusion from equation (6) can be used without considering additional contributions from the thermal gradient in its original form:

$$J_k = -L_{kk}\nabla\left(\frac{\mu_k}{T}\right) \quad (27)$$

which also implies that $J_q^* = J_h$. Excess values, Q_k^* can be accounted for by additional temperature gradient terms, if needed. Partial molar enthalpies, h_k, and partial entropies, s_k, are not currently available from the thermodynamic solver Thermochimica, only the chemical potential, μ_k, is. We are currently implementing methods for calculation of these quantities in the computer library so that they can be used in the above coupled transport equations.

The thermo-diffusion nomenclature varies considerably in the literature. The above terms are taken from reference [29], since they have been used in problems related to nuclear fuels [7, 21]. For more in-depth derivation of the coupled heat and mass transport, textbook [12] is recommended.

4. PARTIAL DIFFERENTIAL EQUATIONS FOR COUPLED MASS AND HEAT TRANSPORT SIMULATIONS

We can now define the governing equations for the problem. The equation for the change of temperature can now be written as an extension of the Fourier equation for heat transport [13]:

$$\frac{d(\rho c_p T)}{dt} + \nabla \cdot J_q'' = P_{\text{heat}} \quad (28)$$

$$P_{\text{heat}} = -\sum_j r_j \nu_j - \sum_k J_k \cdot \nabla u_k + \phi \quad (29)$$

where P_{heat} denote an integral heat source in the volume, and r_j and ν_j denote the heat of reaction and velocity of reaction *j*, respectively, u_k is partial molar energy of the *k*th component, and ϕ denotes an internal heat source, such as fission. The above equations are based on the assumption $J_q^* = J_h$. Accordingly, the enthalpy of the migrating species is accounted for as a heat source on the right-hand side of the equation, and the material properties, conductivity and heat capacity, are based on the starting state of the control volume. Had we used the heat flux definition $J_q^* = J_q''$, the effect of the migrating species on the temperature field would have to be accounted for by the time variation of the heat capacity and conduction. In the next time step, the material parameters need to be updated to the new composition in both formulations.

In the case of nuclear fuel under burnup, the molar enthalpy fluxes of the moving component and the heats of reaction are small compared to the effects of large temperature gradients and the large internal heat generation due to fission, so that we may assume $P_{\text{heat}} = -\phi$. Considering the effect of species transport on the heat equation (28) by incremental material property changes, the heat capacity and heat conduction, is sufficient. Both properties are dependent of the material chemical composition that can be provided by the thermodynamic equilibrium calculations.

Correspondingly, the mass balance equation of diffusing species can be written as:

$$\frac{\partial n_k}{\partial t} = -\nabla \cdot J_k + \sum_j \nu_{kj} v_j = -\nabla \cdot J_k + f_k \quad (30)$$

where v_j and ν_{kj} denote reaction velocity and the corresponding stoichiometric coefficients, respectively. f_k denotes the effective volume of diffusing substance n_k, which for fissioning nuclear fuel is determined from the isotopic inventory and chemical composition calculations [4]. Mass fluxes can be defined based on various formulations above. As stated, the Planck potential form of the driving force would give a form of the equation that would inherently include all the driving forces for mass diffusion. In the cases where the heat of reaction and partial molar enthalpy of the diffusing substance are considerable, they can be included by using the driving forces from equations (20).

5. FEM IMPLEMENTATION OF THE THERMODYNAMIC AND TRANSPORT EQUATIONS

As indicated earlier, coupling the heat and mass transfer balance equations with thermodynamic equilibrium models within the FEM framework involves some practical constrains on the evaluation and integration of the underlying balance equations.

In the FEM models for heat and mass transfer, temperatures and molar densities are the primary variables, and are naturally defined at the finite element nodal points. Assuming the nodes are constitutive volumes of the overall system and they are in local thermodynamic equilibrium, we can calculate chemical potentials using the thermodynamic solver at each node based on the local composition, temperature and pressure. During the integration of the FEM equations, the driving forces for transporting the primary nodal variables (i.e., fluxes) are usually calculated at the integration points. Using $\nabla\left(\frac{\mu_k}{T}\right)$ as the driving force for mass fluxes J_k in the conservation equation is consistent because the Planck potentials are available at the nodes and their gradients are available at the integration points. By the same reasoning, $\nabla\mu_k$, ∇T, ∇n_k, and their various combinations are directly available, as well. Therefore, the diffusion equation can be posed using the gradient of the Planck potential. Most formulations in the literature use $\nabla(\mu_k)_T$ as the driving force, but in the standard FEM element formulations, this value is not well defined at the integration points. Calculating the fluxes and driving forces at FEM integration points from nodal state values corresponds to a Type II process in reference [30]. The finite element integration points (and the finite element itself) are not in local equilibrium, and are used to represent both fluxes and gradients. This gives a more physical interpretation of the non-equilibrium system although creating a philosophical discrepancy by using intensive variables at the points where the equilibrium has not been calculated [31]. In this representation, commonly used in heat and fluid flow analysis, the values of intensive variables and their gradients are assigned to each point within the finite element by interpolation.

Using the volumetric density of a component, n_k, as the primary variable, its flux is defined as the amount of the transported component through a unit area that is normal to the flux direction, over a unit of time. In the Teorell form [32, 33] (mobility × concentration × driving force), the flux is given by a product of volumetric density of the diffusing component, n_k, multiplied by its average constant drift velocity, v_k, normal to the unit area. The International System unit of flux, J_k, with the moles of substance as a measure of the amount of the diffusing matter, is:

$$J_k\left[\frac{\text{mol}}{\text{m}^2\text{s}}\right] = v_k\left[\frac{\text{m}}{\text{s}}\right]\ n_k\left[\frac{\text{mol}}{\text{m}^3}\right] \qquad (31)$$

For uncorrelated movements of the transporting particles with a linear approximation, the drift velocity is a result of the product of the driving forces, F_k, imparted to the unit amount of particles, and the proportionality factor, M_k:

$$v_k = M_k\, F_k \qquad (32)$$

The proportionality factor M_k, termed mobility, is an inverse of the frictional drag of the transporting component experienced by a unit amount of particles as they interact with their environment. The two main types of oxygen transport in UO_2 are by interstitial (in hyper-stoichiometric UO_{2+x}) and vacancy (hypo-stoichiometric UO_{2-x}) diffusion [34]. In the case of interstitial diffusion, interstitial solute oxygen moves between the interstitial sites of the host lattice, UO_2. The defects in the uranium dioxide lattice needed for the transport are controlled by stoichiometry, and, in the case of interstitial diffusion, the

movement is not followed by a countermovement of a defect, such as a vacancy. If the underlying intrinsic mechanism of transport and the mobility for each thermodynamic driving force is the same, then such an interpolation can be further simplified by the use of a common mobility factor.

In the presence of the heterogeneous chemical composition and thermal gradient, the flux expression for species n_k can be written as:

$$J_k \ = -M_k \ n_k F_k = -M_k \ n_k T \nabla \left(\frac{\mu_k}{T}\right) \tag{33}$$

In the case when the concentration of the moving species is given as a fraction of the total amount, such as the site fraction of interstitials, y_i, in the UO_{2+x}, the units in equation (33) are given as:

$$J_k \ \left[\frac{\text{mol}}{\text{m}^2\text{s}}\right] = -M_k \ \left[\frac{\text{mol m}^2}{\text{J s}}\right] y_i \ T[\text{K}] \ \nabla \left(\frac{\mu_k}{T}\right) \left[\frac{\text{J}}{\text{m mol K}}\right] \ n_k \left[\frac{\text{mol}}{\text{m}^3}\right] \tag{34}$$

The integral form of the mass differential conservation equation for implementation in the FEM framework is:

$$\int_V \frac{\partial n_k}{\partial t} \psi \ dV = \int_V J_k \ \nabla \psi \ dV - \int_\Gamma \psi \ J_k \cdot \hat{n} \ \ d\Gamma + \int_V f_k \ \psi \ dV \tag{35}$$

where V and Γ denote the volume and surface of the domain, ψ denotes the test functions, and $\hat{n}$ denotes the outward normal to the domain surface.

In more compact notation, as used in the MOOSE [35] documentation, the integral equation (35) is written as:

$$R(c_k) = \left(\frac{\partial n_k}{\partial t} \ , \psi\right) - \ (\nabla \psi \ , J_k) + \ \langle \psi \ , \ J_k \cdot \ \hat{n} \rangle - \ (\psi \ , f_k) = 0 \tag{36}$$

where parentheses and angled brackets denote corresponding inner products from equation (35) integrated across the domain and over its surface, respectively. In the FEM, the concentration field, n_k, at any location is represented by values at the nodes of a finite element mesh, n_{kj}, and their nodal shape functions, ϕ_j, such that:

$$n_k = \sum_j n_{kj} \phi_j \tag{37}$$

In the FEM formulation used in MOOSE, the test and shape functions are the same. Using equation (37), the residual of equation (36) becomes a vector, $\boldsymbol{R}(\boldsymbol{n_k})$, of the vector of nodal values, $\boldsymbol{n_k}$, and the resulting system of nonlinear equations can be solved using Newton's method by iteratively driving the residual vector to zero. The components of the residual vector are:

$$R_i(\boldsymbol{n_k}) = \left(\frac{\partial \boldsymbol{n_k}}{\partial t} \ , \psi_i\right) - \ (\nabla \psi_i \ , J_k) + \ \langle \psi_i \ , \ J_k \cdot \ \hat{n} \rangle - \ (\psi_i \ , f_k) \ , i = 1, .., N \tag{38}$$

where index *i* denotes the finite element mesh node index associated with the test function ψ_i , and *N* denotes the number of FEM nodes. The elements of the Jacobian matrix, $\mathcal{J}_{ij}$, required for the Newton iterations are:

$$\mathcal{J}_{ij}(\boldsymbol{n_k}) = \frac{\partial R_i\,(\boldsymbol{n_k})}{\partial\, n_{kj}} \tag{39}$$

where indices *i* and *j* denote nodes in the FEM mesh, and n_{kj} denotes a value of $\boldsymbol{n_k}$ at node *j*. The inner products in equation (38) involve derivatives of the mass flux with respect to concentration at node *j*:

$$\left(\nabla\psi_i\,, \frac{\partial J_k}{\partial n_{kj}}\right) \;\;,\;\; \langle\psi_i\,, \frac{\partial J_k}{\partial n_{kj}} \cdot\, \hat{n}\rangle \tag{40}$$

and refer to derivatives of the mass flux in equation for J_k, which are not trivial. MOOSE's Jacobian-Free Newton Krylov (JFNK) solver emphasizes importance of these calculations. Approximate expression for the Jacobian is, nevertheless, necessary in order to achieve a reasonable convergence rate. Using

$$\frac{\partial \boldsymbol{n_k}}{\partial n_{kj}} = \sum_i \frac{\partial}{\partial n_{kj}}(n_{ki}\phi_i) = \phi_j \tag{41}$$

for the mass flux in equation (36), the Jacobian inner product terms can be approximated as:

$$\left(\nabla\psi_i\,, -M_k\, F_k\phi_j\right) \;\;,\;\; \langle\psi_i\,, -M_k\, F_k\phi_j \cdot\, \hat{n}\rangle \tag{42}$$

which omits the partial derivatives of $-M_k$ and F_k .

6. SUMMARY

We have developed thermodynamically and mathematically consistent formulations for coupled mass and heat transport in urania nuclear fuels. The formulations were developed for use in a Finite Element Method application and can be implemented with standard finite element types used in thermal and diffusion simulations. A thermodynamic equilibrium solver provides driving forces, fluxes, material composition and properties based on the isotopic inventory, temperature and pressure. The formulations are implemented into nuclear performance code BISON and demonstrated on the benchmark problems for verification (Appendix).

7. REFERENCES

[1] Olander DR. Fundamental Aspects of Nuclear Reactor Fuel Elements: Technical Information Center, Office of Public Affairs, Energy Research and Development Administration; 1976.
[2] Besmann TM. Computational Thermodynamics: Application to Nuclear Materials. In: Konings RJM, editor. Comprehensive Nuclear Materials: Elsevier; 2012. p. 455 - 70.

[3] Thompson WT, Lewis BJ, Corcoran EC, Kaye MH, White SJ, Akbari F, et al. Thermodynamic treatment of uranium dioxide based nuclear fuel. International Journal of Materials Research. 2007;98:1004-11.
[4] Piro MHA, Banfield J, Clarno KT, Simunovic S, Besmann TM, Lewis BJ, et al. Coupled thermochemical, isotopic evolution and heat transfer simulations in highly irradiated UO2 nuclear fuel. Journal of Nuclear Materials. 2013;441:240-51.
[5] Piro MHA, Simunovic S, Besmann TM, Lewis BJ, Thompson WT. The thermochemistry library Thermochimica. Computational Materials Science. 2013;67:266-72.
[6] Walker CT, Rondinella VV, Papaioannou D, Van Winckel S, Goll W, Manzel R. On the oxidation state Of UO2 nuclear fuel at a burn-up of around 100 MWd/kgHM. Journal of Nuclear Materials. 2005;345:192-205.
[7] Matzke H. Diffusion in Nonstoichiometric Oxides. In: Sorensen TS, editor. Nonstoichiometric Oxides: Academic Press; 1981. p. 155 - 269.
[8] Besmann TM, McMurray JW, Simunovic S. Application of thermochemical modeling to assessment/evaluation of nuclear fuel behavior. Calphad-Computer Coupling of Phase Diagrams and Thermochemistry. 2016;55:47-51.
[9] Lewis BJ, Thompson WT, Iglesias FC. Fission Product Chemistry in Oxide Fuels. In: Konings RJM, editor. Comprehensive Nuclear Materials. "" ed: Elsevier; 2012. p. 515 - 46.
[10] Piro MHA, Simunovic S. Performance enhancing algorithms for computing thermodynamic equilibria. Calphad-Computer Coupling of Phase Diagrams and Thermochemistry. 2012;39:104-10.
[11] Hillert M. Phase Equilibria, Phase Diagrams and Phase Transformations, Their Thermodynamic Basis. 2nd ed. New York: Cambridge University Press; 2007.
[12] Tschoegl NW. Fundamentals of Equilibrium and Steady-State Thermodynamics: Elsevier Science & Technology Books; 2000.
[13] Kondepudi D, Prigogine I. Modern thermodynamics: from heat engines to dissipative structures. 2nd ed: John Wiley & Sons, Ltd; 2015.
[14] Kondepudi D. Introduction to modern thermodynamics: John Wiley & Sons Ltd; 2008.
[15] de Groot SR, Mazur P. Non-Equilibrium Thermodynamics: Dover Publications, Inc.; 2011.
[16] Onsager L. Reciprocal Relations in Irreversible Processes I. Physical Review. 1931;37:405-26.
[17] Piro MHA, Welland MJ, Stan M. On the interpretation of chemical potentials computed from equilibrium thermodynamic codes. Journal of Nuclear Materials. 2015;464:48-52.
[18] Murch GE. Diffusion Kinetics in Solids. In: Kostorz G, editor. Phase Transformations in Materials: Wiley-VCH; 2001. p. 171 - 238.
[19] Lidiard AB. An Essay on the Heat of Transport in Solids and a Partial Guide to the Literature. In: Belova I, Murch G, Öchsner A, editors. Diffusion Phenomena in Engineering Materials2015. p. 57-68.
[20] Janek J, Korte C. Cross effect between heat and matter fluxes in mixed conducting solids - Definition of the heats of transport. Zeitschrift Fur Physikalische Chemie-International Journal of Research in Physical Chemistry & Chemical Physics. 1996;196:187-208.
[21] Janek J, Timm H. Thermal diffusion and Soret effect in (U,Me)O2+delta: the heat of transport of oxygen. Journal of Nuclear Materials. 1998;255:116-27.
[22] Welland MJ. Matter Transport in Fast Reactor Fuels. In: Konings RJM, editor. Comprehensive Nuclear Materials: Elsevier; 2012.
[23] Rahman MA, Saghir MZ. Thermodiffusion or Soret effect: Historical review. International Journal of Heat and Mass Transfer. 2014;73:693-705.
[24] Wurger A. Is Soret equilibrium a non-equilibrium effect? Comptes Rendus Mecanique. 2013;341:438-48.
[25] Raleigh DO, Sommer AW. Thermodynamic Significance of Heat of Transport in Interstitial Solid Solutions. Journal of Chemical Physics. 1962;36:381-&.
[26] Aitken EA. Thermal Diffusion in Closed Oxide Fuel Systems. Journal of Nuclear Materials. 1969;30:62-&.

[27] Norris DIR. Solid-State Transport as a Mechanism of Oxygen Thermomigration in (U,PU) O2+/-X. Journal of Nuclear Materials. 1979;79:118-27.
[28] Grout PJ, Lidiard AB. Computation of heats of transport in crystalline solids: II. Journal of Physics-Condensed Matter. 2008;20.
[29] Allnatt AR, Lidiard AB. Atomic transport in solids: Cambridge University Press; 1993.
[30] Niven RK, Noack BR. Control volume analysis, entropy balance and the entropy production in flow systems. In: Dewar RC, Lineweaver C, Niven RK, Regenauer-Lieb K, editors. Beyond the Second Law: Entropy Production and Non-Equilibrium Systems: Springer-Verlag; 2013. p. 129-62.
[31] Callen HB. Thermodynamics and an Introduction to Thermostatistics. 2nd ed: John Wiley & Sons; 1985.
[32] Teorell T. Transport Processes and Electrical Phenomena in Ionic Membranes. Progress in Biophysics and Biophysical Chemistry. 1953;3:305-69.
[33] Andersson JO, Agren J. Models for Numerical Treatment of Multicomponent Diffusion in Simple Phases. Journal of Applied Physics. 1992;72:1350-5.
[34] Moore E, Gueneau C, Crocombette J-P. Diffusion model of the non-stoichiometric uranium dioxide. Journal of Solid State Chemistry. 2013;203:145-53.
[35] Gaston DR, Permann CJ, Peterson JW, Slaughter AE, Andes D, Wang Y, et al. Physics-based multiscale coupling for full core nuclear reactor simulation. Annals of Nuclear Energy. 2015;84:45-54.
[36] Mihaila B, Stan M, Ramirez J, Zubelewicz A, Cristea P. Simulations of coupled heat transport, oxygen diffusion, and thermal expansion in UO2 nuclear fuel elements. Journal of Nuclear Materials. 2009;394:182-9.
[37] Fink JK. Thermophysical properties of uranium dioxide. Journal of Nuclear Materials. 2000;279:1-18.
[38] Higgs JD, Lewis BJ, Thompson WT, He Z. A conceptual model for the fuel oxidation of defective fuel. Journal of Nuclear Materials. 2007;366:99-128.

APPENDIX A. MOOSE/BISON IMPLEMENTATION OF THE TRANSPORT EQUATIONS

APPENDIX A: MOOSE/BISON IMPLEMENTATION OF TRANSPORT EQUATIONS

The implementation of the oxygen transport formulation in BISON consists of Thermochimica subroutines, MOOSE functions, and MOOSE data structures. The Thermochimica subroutines are used for calculation of thermodynamic parameters that are used for the transport model parameters and driving forces. MOOSE FEM implementation is based on the weak form of conservation equations, namely mass flux and heat diffusion, and on constitutive material models and their parameters. The formulation of the oxygen transport is based on equations (28)-(30). MOOSE functions implemented for this purpose are:

`ThermalUO2PX` (MOOSE Material)
This function implements thermal material model for uranium dioxide as a function of temperature and departure from stoichiometry, x, in $UO_{2\pm x}$. The constitutive material models from [36-38] were used for thermal conductivity, material density and heat capacity. This function couples temperature, material composition, and material heat transport properties.

`OxygenChemistryAux` (MOOSE AuxKernel)
This function calculates thermodynamic parameters required for oxygen transport properties. It uses temperature, pressure and elemental composition at the nodes of the FEM mesh and calculates thermochemical equilibrium. It provides chemical potential of oxygen, Planck potential of oxygen to metal ratio, departure from stoichiometry in $UO_{2\pm x}$, site fraction of oxygen vacancies on the regular anion UO_{2+x} sublattice, site fraction of oxygen interstitials on the oxygen interstitials sublattice [34], and the ratio of the oxygen interstitials to the total oxygen. This function couples the thermodynamic models into parameters used in the heat and mass transport models.

`MobilityUOX` (MOOSE Material)
This function calculates mobility parameter for uranium oxide based on reference [34]. It uses site fractions of oxygen vacancies and interstitials as calculated in `OxygenChemistryAux`. It also couples the temperature field from the heat diffusion calculation.

`ChemicalDiffusion` (MOOSE Kernel)
This kernel uses the gradient in oxygen chemical potential from `OxygenChemistryAux` as the driving force for the oxygen flux. The oxygen chemical potential gradient is multiplied by the oxygen mobility calculated in `MobilityUOX`, and by the concentration of oxygen multiplied by the ratio of the concentration of oxygen in the interstitial lattice and the total oxygen concentration. The main variable for this kernel is the total concentration of oxygen.

`ChemicalDiffusionPlanck` (MOOSE Kernel)
This kernel uses gradient of oxygen Planck potential from `OxygenChemistryAux` as the driving force for the oxygen flux. The oxygen Planck potential gradient is multiplied by the oxygen mobility calculated in `MobilityUOX`, temperature and the concentration of oxygen multiplied by the ratio of the concentration of oxygen in the interstitial lattice and the total oxygen concentration. The main variable for this kernel is the total concentration of oxygen.

The relation between the BISON functions used for the transport simulation is shown in Table A.1. For each function, the list of input (In) and updated (Out) variables determines the function's dependency on other functions.

Table A1. Relation between functions and variables in the oxygen transport simulation.

Function	Variables	
`ThermalUO2PX`	In	x, $\boldsymbol{T}$
	Out	k, C_p, ρ
`MobilityUO2`	In	y_{Va} , y_{Io} , $\boldsymbol{T}$
	Out	M_O
`OxygenChemistryAux`	In	U , $\boldsymbol{O}$, $\boldsymbol{T}$
	Out	y_{Va} , y_{Io} , x , μ_O , μ_O/T, $O_{Io}/\boldsymbol{O}$
`HeatConduction`	In	k , T
	Out	T
`HeatConduction TimeDerivative`	In	k, , C_p, ρ, T
	Out	T
`ChemicalDiffusion`	In	$\boldsymbol{O}$, μ_O , μ_O/T , M_O, O_{Io}/O
	Out	$\boldsymbol{O}$
`ChemicalDiffusionPlanck`	In	$\boldsymbol{O}$, μ_O , μ_O/T , M_O, O_{Io}/O
	Out	$\boldsymbol{O}$
`TimeDerivative`	In	$\boldsymbol{O}$
	Out	$\boldsymbol{O}$

Symbols in Table A1: U – total concentration of uranium atoms, O – total concentration of oxygen atoms, k – thermal conductivity, C_p – heat capacity, ρ – mass density, T – temperature, y_{Va} - site fraction of oxygen vacancies on the regular anion sublattice, y_{Io} - site fraction of oxygen interstitial atoms, μ_O - chemical potential of oxygen, μ_O/T – oxygen Planck potential, O_{Io} – concentration of oxygen interstitial atoms. Primary variables are denoted by boldface. The U-O system u is used only for illustration. More complex systems can be modeled by using a larger elemental inventory as produced during burnup.

APPENDIX B. TEST EXAMPLES

APPENDIX B: TEST EXAMPLES

B.1 TEST EXAMPLE FOR THERMODYNAMIC CALCULATIONS

A unit cube problem has been set up in BISON's `tests/oxygen_dg` directory for case study of parameter and material model calculations in `OxygenChemistryAux`, `ThermalUO2PX` and `MobilityUOX` functions. A simple uranium-oxygen material system with 1 mole of uranium and 2.05 moles of oxygen has been used. The nominal oxygen-to-metal ratio in this system is, therefore, 2.05. The oxygen-to-metal ratio on the fluorite lattice depends on temperature, and pressure. First, standalone Thermochimica calculations were performed for the given composition and varying temperatures. The results were compared against reference [34]. The results are shown in the figures below.

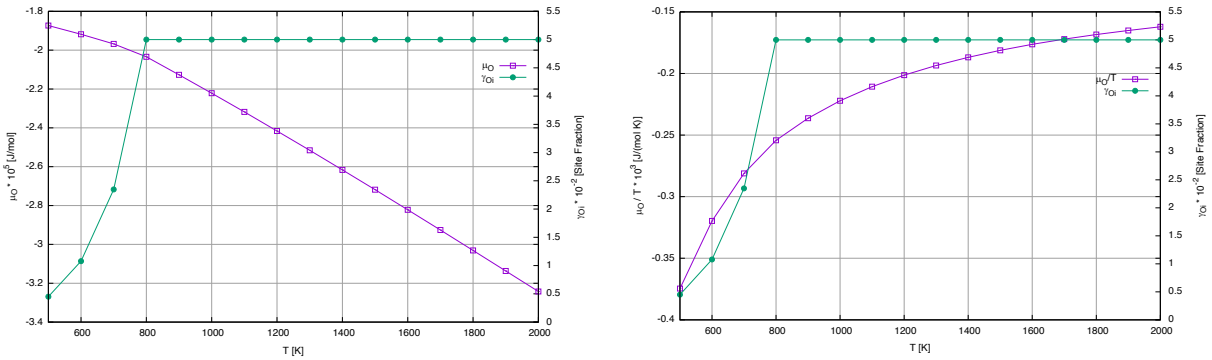

(a) (b)

Figure B1: Variation of (a) chemical $\nabla\mu_k$ and, (b) Planck potential of oxygen $\nabla\left(\frac{\mu_k}{T}\right)$ and site fraction of oxygen interstitials on fluorite lattice for composition of 1 mol U, and 2.05 mol O.

The results in Figure B1 were used as a benchmark for BISON simulation of material parameter evolution in a unit cube under a temperature gradient. The material had the same composition and the thermodynamic models as the point calculations in Figure B1. Material models were based on property models from reference [36]. The results of BISON simulations are shown in figures below.

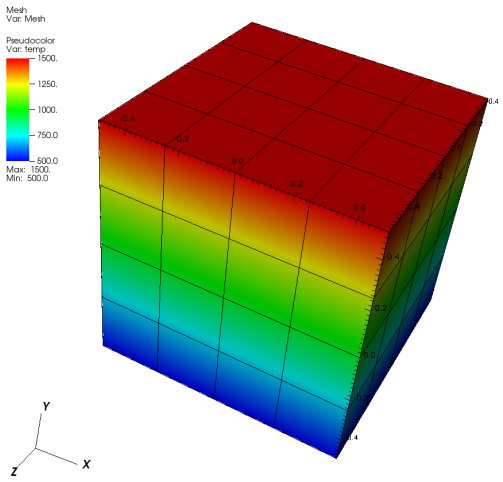

Figure B2: Steady state temperature for the test problem with composition of 1 mol U, and 2.05 mol O.

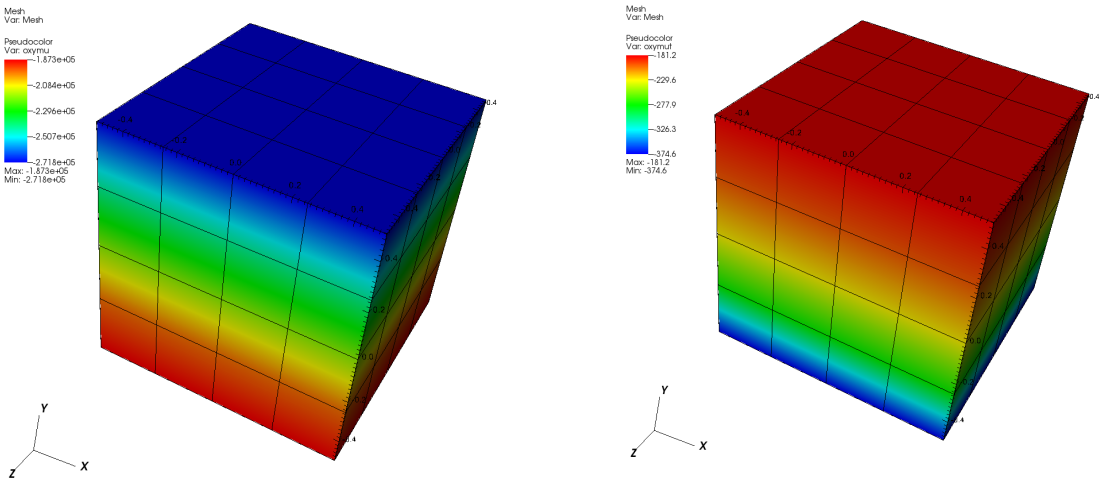

(a) (b)

Figure B3: Steady state (a) oxygen chemical potential and (b) oxygen Planck potential distributions for the test problem with composition of 1 mol U, and 2.05 mol O.

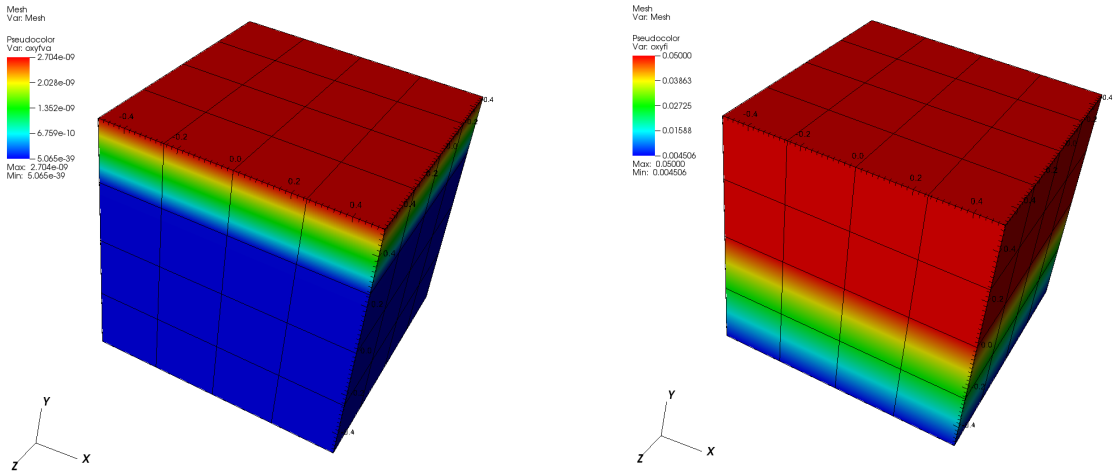

(a) (b)

Figure B4: Steady state distributions (a) site fractions of the oxygen vacancies on the regular anion lattice and (b) site fractions of the oxygen interstitials on the interstitial lattice for the test problem with composition of 1 mol U, and 2.05 mol O.

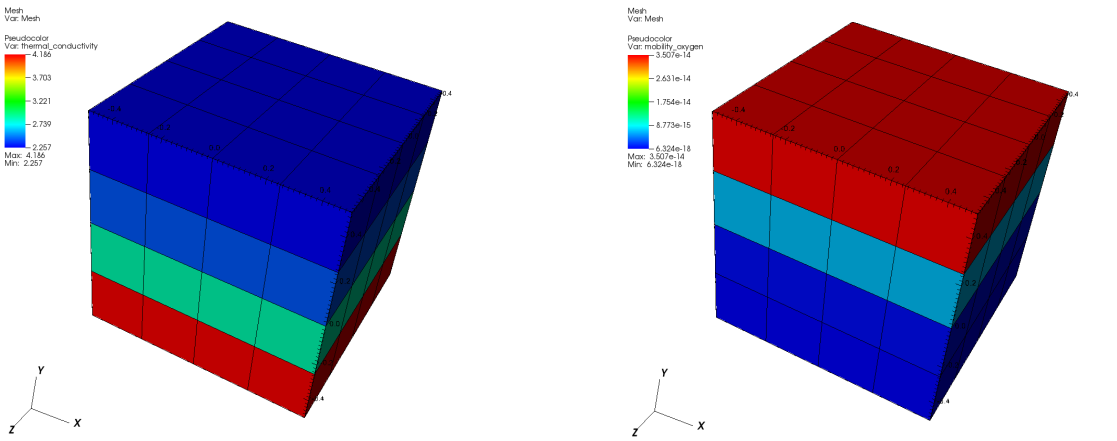

(a) (b)

Figure B5: Steady state distributions of (a) thermal conductivity and (b) mobility of oxygen for the test problem with composition of 1 mol U, and 2.05 mol O.

B.2 TEST EXAMPLE FOR OXYGEN TRANSPORT MODEL

A simple example problem has been set up to validate the developed functions for oxygen transport. The example is in BISON's `tests/oxygen_chemdiffusionplanck` directory. The domain of the example is a prism with dimensions of 2 cm x 1 cm x 1 cm. An initial composition of 1 mol of U and 2.1 moles of oxygen have been used at constant temperature of 1400 K. Temperature boundary conditions are suddenly changed to create a gradient in temperature along the dominant dimension. The oxygen is transported due to a driving force resulting from the oxygen Planck potential gradient that is established by the temperature differential. We have not applied the transformation of the existing experimental parameters for the isothermal diffusion coefficients to the form using the Planck potential so that the current results are only illustration of the method. Figure B6 shows the steady state temperature field in the prism and the oxygen distribution.

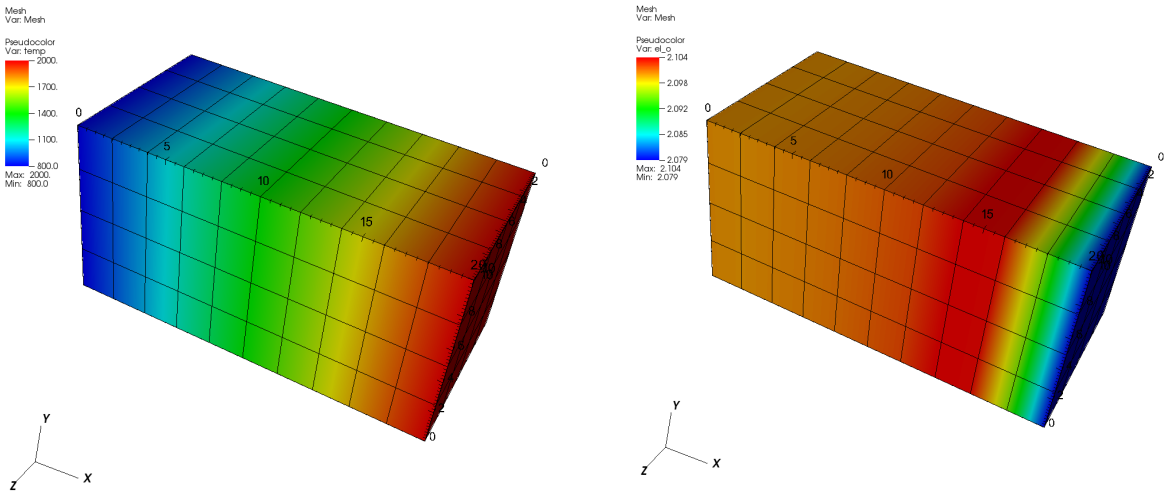

(a) (b)

Figure B6: (a) Temperature and (b) oxygen distributions at the end of simulation.

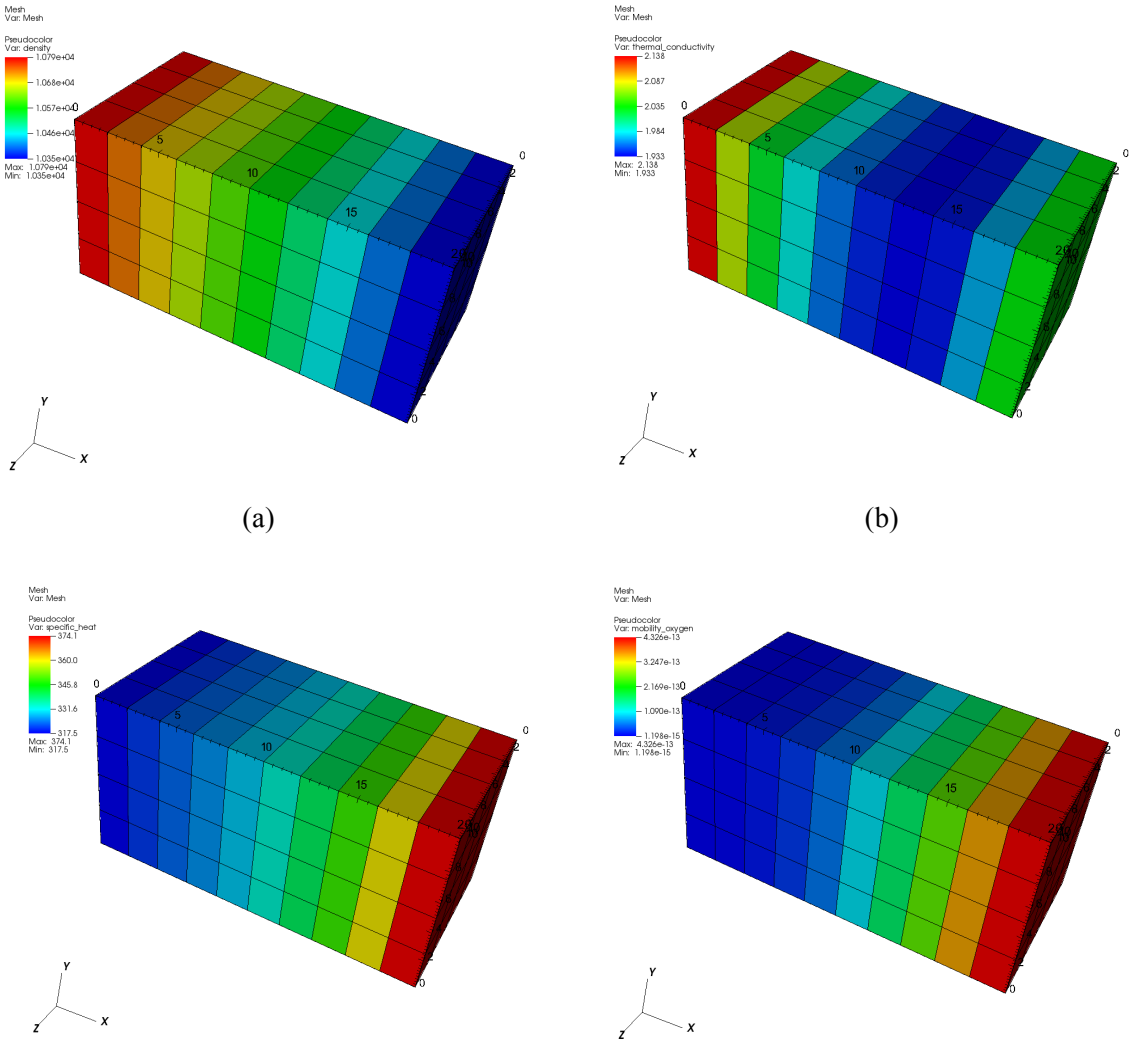

Figure B7: Material properties (a) density, (b) conductivity, (c) specific heat, (d) oxygen mobility.

The distributions of site fractions for the oxygen vacancies and oxygen interstitials are shown in Figure B8.

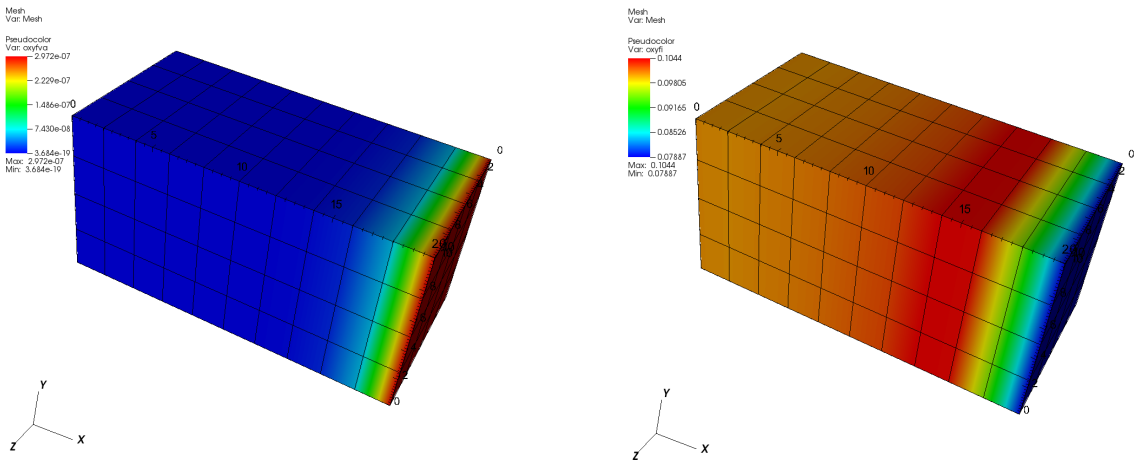

(a) (b)

Figure B8: Distribution of (a) site fraction of oxygen vacancies on the anion lattice, and (b) oxygen interstitials.